Hindawi
Mathematical Problems in Engineering
Volume 2018, Article ID 5021245, 9 pages
https://doi.org/10.1155/2018/5021245

Research Article

Modal Analysis of a Thick-Disk Rotor with Interference Fit Using Finite Element Method

Yuhua Fan, Hongchang Ding, Maoyuan Li, and Jiacheng Li

School of Mechanical and Electronic Engineering, Shandong University of Science and Technology, Qingdao, 266590, China

Correspondence should be addressed to Hongchang Ding; dhchang@163.com

Received 9 June 2018; Revised 14 September 2018; Accepted 25 September 2018; Published 14 October 2018

Academic Editor: Stylianos Georgantzinos

This paper is concerned with the modal analysis of a thick-disk rotor, which consists of an elastic shaft with a rigid thick disk assembled by interference fit, and the width of the thick disk is not negligible. Firstly, the friction moment on the contact surface of disk and shaft is deduced in terms of elastic theory, and a new enhanced coefficient of bending stiffness of assembly body is proposed and calculated for the first time. Secondly, the effect of the width of thick disk on diametrical moment of inertia, as well as the enhanced coefficient of bending stiffness of interference-fit part between disk and shaft, is included in the motion equations of thick-disk rotor, which are established based on finite element method, and the natural frequencies of rotor are obtained by solving the motion equations. Then the modal analysis is performed to get the natural frequencies in ANSYS Workbench, in which the friction coefficient and interference fit are set to be the same as those of the finite element calculation method. At last the modal experiment is done to verify the accuracy of calculation and simulation. The results show that the calculation values using enhanced stiffness of assembly part are in good agreement with those of ANSYS Workbench and experiment, and the percent errors of the first natural frequency and the second natural frequency are down to about 0.32% and 0.83%, respectively.

1. Introduction

Rotor is the key component of rotating machinery, which is widely used in mechanical devices including gas turbines, aeroengines, industrial compressors, and motors etc., and the accurate prediction of natural frequencies of rotor is important for the safe operation of rotating machineries. There are many studies on dynamic analysis of rotor system for the solution of critical speeds and natural frequencies. In the studies by Nelson and Zorzi et al. [1, 2], dynamic analysis of rotor system was investigated based on finite element method, and the critical speeds were calculated, which included the effect of various parameters such as rotary inertia, gyroscopic moment, and internal damping. Ku et al. [3] developed a Timoshenko beam finite element model and studied the combined effects of shear deformations and internal damping on forward and backward whirl speeds. Kalita et al. [4] and Chouksey et al. [5] analyzed the effect of fluid film bearing on whirl speeds of rotor-bearing system and found that a half whirl exists in the rotation caused by hydrodynamic bearings. In addition, Lee et al. [6] investigated two different approaches (Floquet theory and coordinate transformation) to develop the complex modal analysis for periodically time-varying linear rotor systems and found that the results of coordinate transformation are much efficient. Khulief et al. [7] investigated the modal characteristics of complex rotor-bearing systems using finite element method and came to the conclusion that the results including the rotational effects were more accurate. Forrai [8] dealt with the stability analysis of self-excited bending vibrations of linear symmetrical rotor-bearing systems with internal damping.

In the establishment of the above finite element model of single-disk rotor or complex rotor system, the width (or thickness) of rotor disk is usually neglected, and the bending stiffness of interference-fit part between disk and shaft equals the stiffness of shaft. In fact, the width of thick disk of rotor has an obvious effect on the diametrical moment of inertia of disk and bending stiffness of interference-fit part, which will change the calculation accuracy of natural frequencies of rotor system.

Liu et al. [9] analyzed the transient vibration of a single thick-disk rotor, whose radial moment of inertia of disk

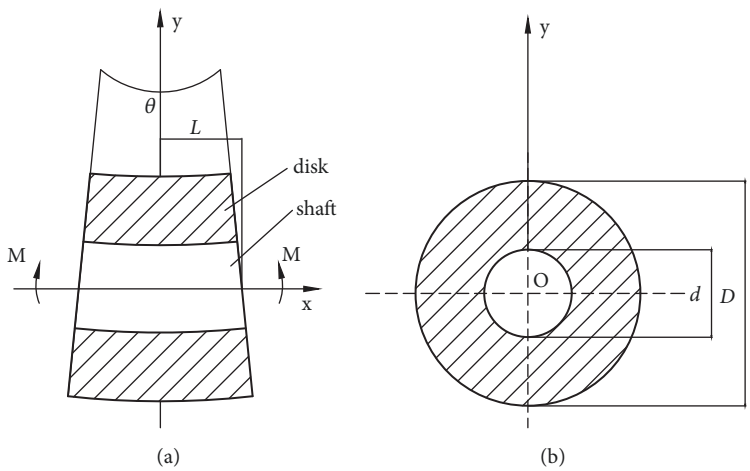

Figure 1: Mechanical model of disk shaft under external bending moment. (a) Axial plane view of model and (b) cross section view of model.

was bigger than the axial one. Pan et al. [10] studied the influence of quality and position of disk on critical speeds of rotor system, which was verified by theoretical calculation and experiment. Petrescu et al. [11] concluded the mass moments of inertia corresponding to different geometric shapes, objects, and profiles. Chen et al. [12] studied the influence of a hot-fit rotor on the local stiffness of the hollow shaft and obtained the accurate natural frequencies using contact elements. Huang et al. [13] optimized the contact stiffness factor of flexible rotor system of magnetic levitation motors and obtained the very close results of natural frequencies by ANSYS Workbench and modal experiment. Kim et al. [14] analyzed the forced vibration of a Timoshenko beam subjected to stationary and moving loads using the modal analysis method. Jalali et al. [15] performed the dynamic analysis of a high speed rotor-bearing system and got the natural frequencies and mode shapes of the rotor at rest under free-free boundary conditions. Giannopoulos et al. [16] analyzed the local flexibility of a shaft with a breathing crack, which is reciprocal of stiffness. In addition, the influences of normal contact stiffness on vibration modes of rod fastening rotors were studied and analyzed in [17, 18].

In this study, the modal characteristics of a thick-disk rotor with interference fit is analyzed, whose radial moment of inertia of disk is smaller than the axial one. The friction moment of contact surfaces between disk and shaft is firstly deduced based on elastic theory, and the enhanced coefficient of bending stiffness of thick disk on shaft is proposed and calculated. Then the finite element motion equation of the thick-disk rotor is established, and the enhanced coefficient of stiffness and effect of thick-disk width on diametrical moment of inertia are included in the solution of motion equation for natural frequencies. In addition, the modal analysis is performed on ANSYS Workbench for the verification of calculation results, and the friction coefficient is set to be in accordance with that of finite element calculation. At last the modal experiment is carried out by the application of LMS Test.Lab, and the experiment results are in good agreement with those of theoretical calculation and ANSYS Workbench containing enhanced stiffness of assembly part. The research results not only provide a theoretical basis for the modal analysis of thick-disk rotor with interference fit, but also are suitable for the accurate calculation of natural frequencies of other rotors with interference fit.

2. Calculation of Friction Moment and Enhanced Coefficient of Bending Stiffness

2.1. Friction Moment. The mechanical model of disk-shaft assembly body is shown in Figure 1, in which the disk and shaft are assembled by interference fit. When the assembly body is subject to external bending moment, the bending of assembly body will produce friction moment on the contact surfaces because of the relative sliding of disk against shaft. In Figure 1, θ is the bending angle of assembly body, M is the external bending moment, L is half of the width of assembly body, d is the internal diameter of hollow disk, which is equal to the diameter of shaft, R_0 is the radius of shaft (d=2R_0), and D and R_2 are the external diameter and radius of hollow disk (D=2R_2), respectively.

For the convenience of calculation and analysis, the dimensionless parameters are supposed to be as follows:

$$\begin{aligned} \overline{D} &= \frac{R_2}{R_0} = \frac{D}{d}, \\ \overline{B} &= \frac{L}{R_0}, \\ \overline{C} &= \frac{\delta}{d}, \\ \xi &= \frac{x}{L} \end{aligned} \tag{1}$$

where δ is the magnitude of interference fit along diameter direction, x is a coordinate point of assembly body in x-axis direction, and ξ is the dimensionless parameter corresponding to x.

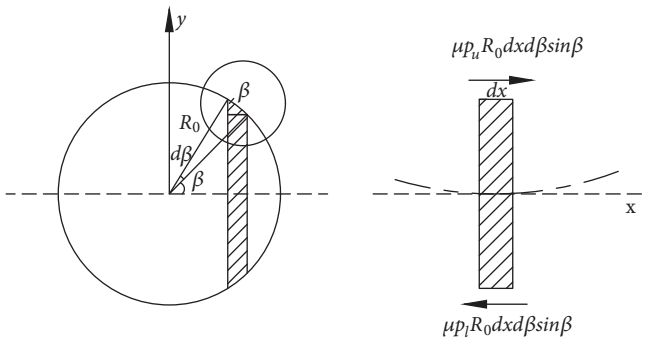

Figure 2: Friction moment on contact surfaces.

The bending stiffness (EI_c) of assembly body is expressed as

$$EI_c = EI_1 k\left(\overline{D}, \overline{B}, \overline{C}\right) \tag{2}$$

where E is the elastic modulus of disk and shaft material, I_c is the equivalent section moment of inertia of assembly body, I_1 is the section moment of inertia of shaft, and $k(\overline{D}, \overline{B}, \overline{C})$ is the enhanced coefficient of bending stiffness, which depends on the dimensionless parameters $\overline{D}, \overline{B}, \overline{C}$.

According to Lame equation [19, 20], the interference fit between disk and shaft can be expressed as

$$\delta = \frac{d \cdot p}{E} \cdot \frac{2D^2}{D^2 - d^2} \tag{3}$$

where p is the compressive stress on the contact surfaces of disk and shaft, which is produced by interference fit.

Substituting Eq. (1) into Eq. (3), the compressive stress can be obtained as

$$p = \frac{1}{2} \cdot \frac{\overline{D}^2 - 1}{\overline{D}^2} \cdot \frac{E}{R_0} \cdot \frac{\delta}{2} \tag{4}$$

The pressure of upper and lower contact surfaces between shaft and disk are expressed as

$$p_u(\xi) = \frac{1}{2} \cdot \frac{\overline{D}^2 - 1}{\overline{D}^2} \cdot \frac{E}{R_0} \cdot \left(\frac{\delta}{2} + S(\xi)\right) \cdot \sin\beta \tag{5}$$

$$p_l(\xi) = \frac{1}{2} \cdot \frac{\overline{D}^2 - 1}{\overline{D}^2} \cdot \frac{E}{R_0} \cdot \left(\frac{\delta}{2} - S(\xi)\right) \cdot \sin\beta \tag{6}$$

where $S(\xi)$ is the variation of interference fit in radius direction as the assembly body is bent under external moment and p_u, p_l are the pressure of the upper and lower contact surface, respectively. Multiplication coefficient $\sin\beta$ represents p_u and p_l which are the contact pressure component of y direction and the contact pressure component of x direction, which can cancel each other out.

Figure 2 shows the friction moment on the contact surfaces. In Figure 2, $R_0 dx d\beta$ represents unit area of shaft surface, and the multiplication coefficient $\sin\beta$ represents the unit area perpendicular to the pressures p_u and p_l. When the assembly body of disk and shaft is bent under external bending moment, there will be the trend of relative sliding on the contact surfaces, and it is supposed that μ is the friction coefficient of contact surfaces, so $\mu p_u R_0 dx d\beta$ and $\mu p_l R_0 dx d\beta$ are the produced friction forces on the unit area of upper or lower contact surfaces, and they can be expressed as

$$dF_u = \mu p_u R_0 dx d\beta \sin\beta \tag{7}$$

$$dF_l = \mu p_l R_0 dx d\beta \sin\beta \tag{8}$$

From the integral of Eqs. (7) and (8), the friction forces can be expressed as follows:

$$F_u = \int_0^{\pi} \int_0^{L} \mu p_u R_0 \sin\beta dx d\beta \tag{9}$$

$$F_l = \int_0^{-\pi} \int_0^{L} \mu p_l R_0 \sin\beta dx d\beta \tag{10}$$

So the friction moment can be written

$$M_\mu = \left(F_u + F_l\right) \cdot R_0 \tag{11}$$

Substituting Eqs. (9) and (10) into Eq. (11) and solving the integral of Eq. (11) along x axis, the friction moment M_μ can be obtained as follows:

$$M_\mu = \frac{1}{2}\pi\mu E \overline{B}\,\overline{C} R_0^{\,3}\left(1 - \overline{D}^{-2}\right) \tag{12}$$

2.2. Enhanced Coefficient of Bending Stiffness. In Figure 1, the bending angle of shaft is expressed as

$$\theta = \frac{ML}{EI} \tag{13}$$

The maximum external bending moment of shaft occurs when the stress of cross section reaches yield stress

$$M_\sigma = \frac{I \cdot \sigma_s}{R} \tag{14}$$

where M_σ is the maximum external bending moment, R is the radius of shaft, and σ_s is the yield stress of shaft material.

Then the external bending moment can be expressed as

$$M = \alpha \cdot M_\sigma \tag{15}$$

where the coefficient α satisfies the condition $0 < \alpha \leqslant 1$.

To bend the assembly body of disk and shaft, extra external bending moment is needed to overcome the friction moment, so Eq. (13) can be expressed as

$$\theta = \frac{ML}{EI_c} = \frac{\left(M + M_\mu\right)L}{EI_1 k\left(\overline{D}, \overline{B}, \overline{C}\right)} \tag{16}$$

According to Eqs. (12), (15), and (16), the enhanced coefficient of bending stiffness can be obtained as follows:

$$k\left(\overline{D}, \overline{B}, \overline{C}\right) = 1 + \frac{2\mu E \overline{B}\,\overline{C}\left(1 - \overline{D}^{-2}\right)}{\sigma_s \alpha} \tag{17}$$

where the enhanced coefficient depends on the parameters such as friction coefficient, yield stress, Young's modulus, $\overline{D}$, $\overline{B}$, $\overline{C}$ etc.

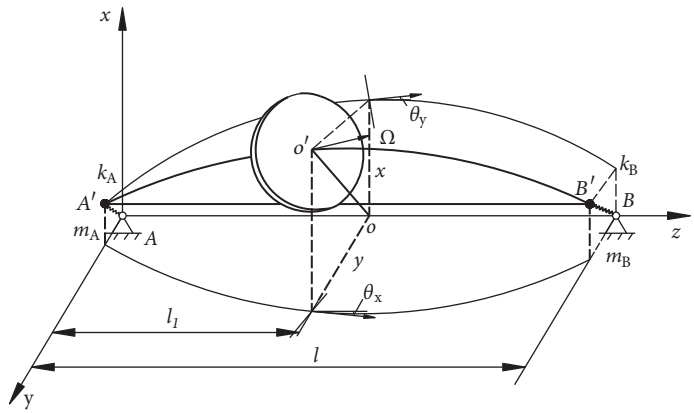

Figure 3: Model of single disk rotor system.

3. Motion Equation of Rotor System

The mathematical model of rotor system is composed of single rigid thick disk, flexible shaft, and bearings, which is illustrated in Figure 3.

3.1. Rigid Thick Disk. In Figure 3, the displacement vector of disk is given by

$$u_{1d} = \left\{x, \theta_y\right\}^T;$$
$$u_{2d} = \left\{y, -\theta_x\right\}^T \tag{18}$$

And the motion equation of the rigid disk is expressed as

$$[M_d]\{\ddot{u}_{1d}\} + \Omega[J_d]\{\dot{u}_{2d}\} = \{Q_{1d}\}$$
$$[M_d]\{\ddot{u}_{2d}\} - \Omega[J_d]\{\dot{u}_{1d}\} = \{Q_{2d}\} \tag{19}$$

where Ω is the spin angular velocity of disk, Q_d is the vector of generalized forces, and M_d and J_d are mass matrix and gyroscopic matrix, respectively, which are defined as

$$[M_d] = \begin{bmatrix} m & 0 \\ 0 & J_t \end{bmatrix} \tag{20}$$

$$[J_d] = \begin{bmatrix} 0 & 0 \\ 0 & J_p \end{bmatrix} \tag{21}$$

where m is the mass of disk and J_t and J_p are diametrical and polar moments of inertia of disk, respectively.

When the width of thick disk is included in the calculation of moment of inertia as in Figure 4, the diametrical and polar moments of inertia of thick disk can be expressed as follows: [11]

$$J_p = \frac{1}{2}m\left(r_i^2 + r_e^2\right) \tag{22}$$

$$J_t = \frac{1}{4}m\left(r_i^2 + r_e^2\right) + \frac{1}{12}mb^2 \tag{23}$$

where r_e, r_i are the external and inner radius of thick disk, respectively, and b is the width of thick disk.

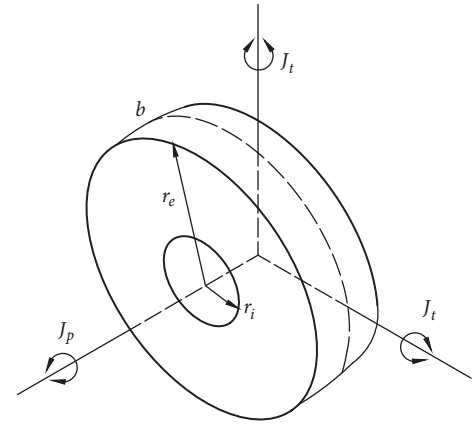

Figure 4: Moment of inertia of thick disk.

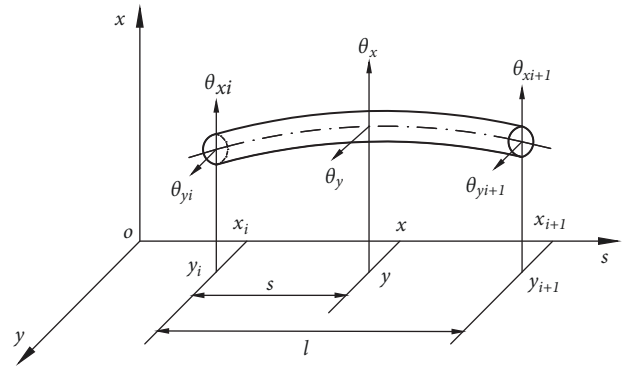

Figure 5: Shaft finite element.

3.2. Shaft Finite Element. The shaft finite element has eight degrees of freedom, and it is defined by two nodes, as shown in Figure 5. Its parameters are denoted as follows: l is the length of the shaft element, S is the area of the cross section of the shaft element, J_{SD} and J_{SP} are diametrical and polar moments of inertia of shaft element, and E, ρ are the Young's modulus and density of the shaft material, respectively.

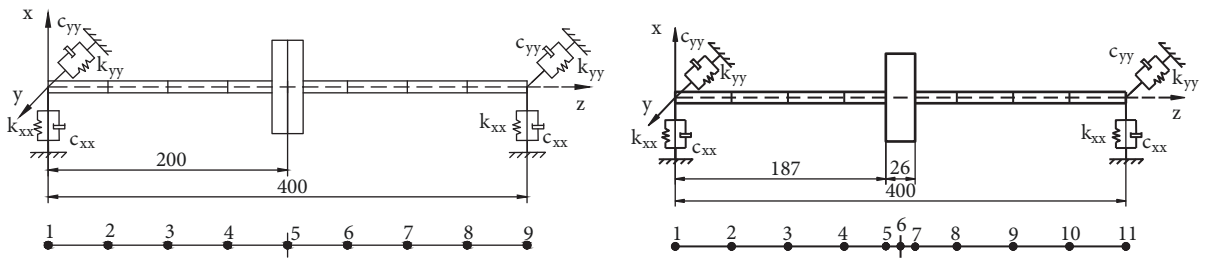

(a) Finite element structure of 9 nodes

(b) Finite element structure of 11 nodes

Figure 6: Finite element structure of thick-disk rotor.

The nodal displacement vector of the ith shaft element is given by

$$u_{1s} = \left\{x_i, \theta_{yi}, x_{i+1}, \theta_{yi+1}\right\}^T;$$
$$u_{2s} = \left\{y_i, -\theta_{xi}, y_{i+1}, -\theta_{xi+1}\right\}^T \tag{24}$$

When the rotor shaft is discretized into "N" finite elements, the total number of nodes becomes "N+1". And the motion equation of the shaft finite element without internal viscous damping can be expressed as [1, 2, 5]:

$$\begin{aligned}\left[M_{ST} + M_{SR}\right]\left\{\ddot{u}_{1S}\right\} + \Omega\left[J_S\right]\left\{\dot{u}_{2S}\right\} + K_S\left\{u_{1S}\right\} &= \left\{Q_{1S}\right\}\\ \left[M_{ST} + M_{SR}\right]\left\{\ddot{u}_{2S}\right\} - \Omega\left[J_S\right]\left\{\dot{u}_{1S}\right\} + K_S\left\{u_{2S}\right\} &= \left\{Q_{2S}\right\}\end{aligned} \tag{25}$$

where M_{ST}, M_{ST}, J_S are the mobile mass matrix, rotating mass matrix, and moment of inertia, respectively, and K_S is the stiffness of shaft element, which is written as

$$\left[K_S\right] = \frac{EI}{l^3}\begin{bmatrix} 12 & 6l & -12 & 6l \\ 6l & 4l^2 & -6l & 2l^2 \\ -12 & -6l & 12 & -6l \\ 6l & 2l^2 & -6l & 4l^2 \end{bmatrix} \tag{26}$$

The enhanced stiffness of the assembly part of shaft will be enhanced for the shrink fit of thick disk; according to Eqs. (2) and (17), the enhanced stiffness can be got as follows:

$$\left[K_s{}'\right] = k\left(\overline{D}, \overline{B}, \overline{C}\right)\left[K_s\right] \tag{27}$$

3.3. Bearings. The linear isotropic damped bearings can be modeled by the equation

$$\left[C_{brg}\right]\left\{\dot{u}_b\right\} + \left[K_{brg}\right]\left\{u_b\right\} = \left\{Q_b\right\} \tag{28}$$

where u_b is the displacement vector at the bearing location, Q_b is the bearing force vector, and subscript "brg" represents the bearing. And the damping and stiffness matrices of bearings are defined as

$$C_{brg} = \begin{bmatrix} c_{xx} & c_{xy} \\ c_{yx} & c_{yy} \end{bmatrix},$$
$$K_{brg} = \begin{bmatrix} k_{xx} & k_{xy} \\ k_{yx} & k_{yy} \end{bmatrix} \tag{29}$$

where subscript "xx" represents x direction, "yy" represents y direction, and "xy" and "yx" represent the couple direction of x and y.

3.4. Motion Equation of Rotor System. Based on Eqs. (19), (25), and (28), the motion equation of the rotor-bearing system can be written as follows:

$$[M]\{\ddot{u}\} + [C]\{\dot{u}\} + [K]\{u\} = \{Q\} \tag{30}$$

For the solution of natural frequencies and mode shapes of rotor, the external force and damping can be ignored, and Eq. (30) becomes the free motion equation of thick-disk rotor as follows:

$$[M]\{\ddot{u}\} + [K]\{u\} = 0 \tag{31}$$

where the stiffness matrix K has included the enhanced stiffness.

It is supposed that the solution of Eq. (31) is as follows: $u = U\exp(j\omega t)$, and the characteristic equation can be got as follows:

$$\left(K - \omega^2 M\right)U = 0 \tag{32}$$

In Eq. (32), as not all amplitudes are equal to zero for free vibration rotor, the only condition for nonzero solution is that the coefficient of the determinant is equal to zero.

$$\left|K - \omega^2 M\right| = 0 \tag{33}$$

Then the characteristic values of Eq. (33) are the natural frequencies of rotor, and the nonzero vectors of Eq. (32) respond to the corresponding vibration modes.

4. Calculation of Natural Frequencies and Modal Analysis

4.1. Calculation of Natural Frequencies. The calculation model of a thick-disk rotor is made up of disk and shaft via an interference fit, and the structural parameters of the thick-disk rotor are shown in Table 1.

The finite element structure of the thick-disk rotor is shown in Figure 6. As shown in Figure 6(a), there are 9 nodes and the mass of disk acts on node 5; the stiffness matrix of thick-disk rotor is equal to the stiffness of shaft, so the

Table 1: Structure parameters of thick-disk rotor.

Name	Value
Diameter of thick disk (mm)	76
Width of thick disk (mm)	26
Diameter of shaft (mm)	10
Length of shaft (mm)	400
Material	40Cr
Density, ρ (kg/m^3)	7850
Modulus of elasticity, E (Pa)	2×10^{11}
Poisson ratio, γ	0.3
Magnitude of interference, δ (mm)	0.05
Friction coefficient, μ	0.02

Table 2: Natural frequencies of thick-disk rotor.

	1st Flexural	2nd Flexural
9 nodes (no enhanced stiffness)	189.25 Hz	479.07 Hz
11 nodes (enhanced stiffness)	199.13 Hz	494.20 Hz

model solution is not affected by the enhanced coefficient of stiffness, and the results will be the same with those of conventional thin-disk rotor. In Figure 6(b), the rotor is discretized into 11 nodes, the mass of disk acts on node 6, and the enhanced coefficient of stiffness is taken into account in the model establishment, so the stiffness of shaft between nodes 5 and 7 should multiply the enhanced coefficient for the solution of natural frequencies according to Eq. (27).

By solving Eq. (33), the natural frequencies of thick rotor are obtained using the parameters in Table 1, and the calculation results are shown in Table 2. Comparing the natural frequencies of 9-node rotor with those of 11 nodes, it can be seen that the natural frequencies are greatly influenced by the enhanced coefficient of stiffness, and the percent error of first frequency is about 5.22%, and the second is about 3.15%.

4.2. Modal Analysis of Thick-Disk Rotor in ANSYS Workbench. The 3D finite element solid model of thick-disk rotor is established in ANSYS Workbench, as shown in Figure 7. The finite element grid of rotor model is automatically generated, and the calculating model contains 2908 nodes and 526 units. By contrast, the natural frequencies obtained in ANSYS Workbench will be more accurate than those by finite element calculation.

The influence of interference fit of thick disk and shaft on stiffness is included in the ANSYS Workbench. So the contact mode is set to be of frictional type in ANSYS Workbench, and the magnitude of interference fit and friction coefficient are set to be in accordance with those of theoretical finite element calculation as in Table 1. In addition, the contact stiffness should be considered in ANSYS Workbench, and the conventional value is from 0.01 to 0.1 for bending analysis. When the contact stiffness is set to be 0.01, solving the model in ANSYS Workbench, the modal shape of the first

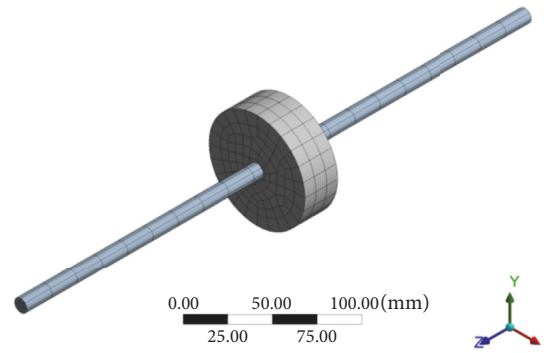

Figure 7: Finite element grid of rotor.

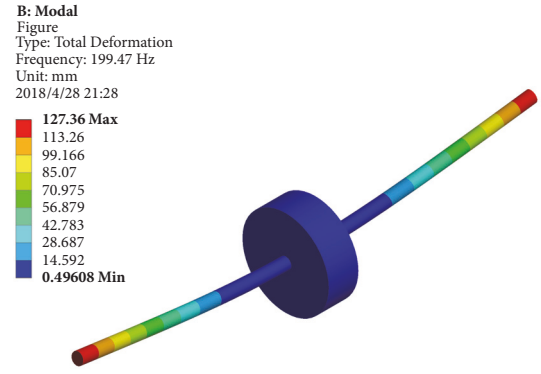

(a) First natural frequency (199.47Hz)

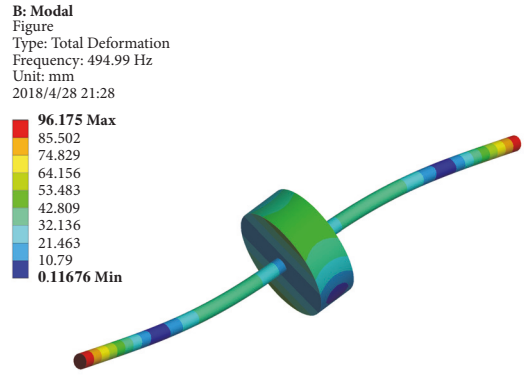

(b) Second natural frequency (494.99Hz)

Figure 8: Modal shape of thick-disk rotor.

two natural frequencies of the thick-disk rotor is obtained as shown in Figure 8. It can be seen that the first two natural frequencies of the rotor are f_1=199.47Hz, f_2 =494.99Hz, respectively. When the contact stiffness is equal to 0.1, the first two natural frequencies are f_1=203.31Hz, f_2 =499.39Hz. All the results obtained in ANSYS Workbench are very close to those of theoretical finite element calculation with enhanced stiffness.

To compare the enhancement of thick disk on the bending stiffness of shaft in ANSYS Workbench, another 3D model is established, as shown in Figure 9. The mass of thick disk is

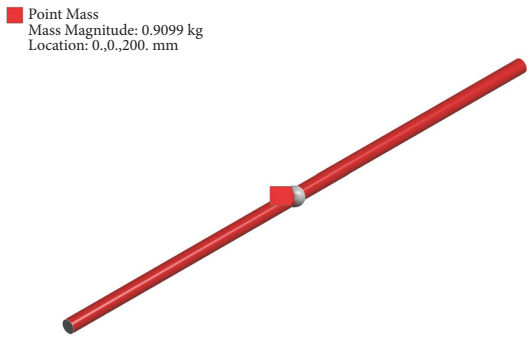

Figure 9: Rotor model with shaft and single mass point.

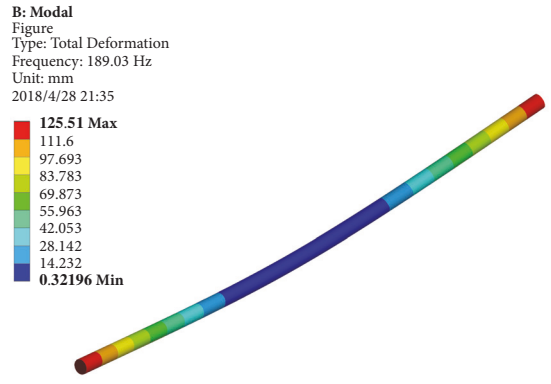

(a) First natural frequency (189.03Hz)

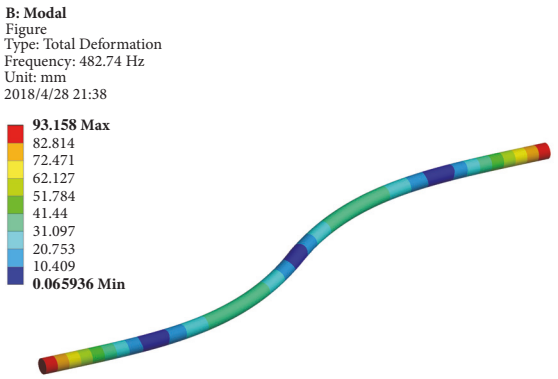

(b) Second natural frequency (482.74Hz)

Figure 10: Modal shape of rotor with shaft and single mass point.

simplified to a point, which is applied at the middle point of the rotating shaft, and the mass and moment of inertia of this point are exactly equal to those of the thick disk. Compared to the solid model in Figure 8, the modal solution is not subject to the influence of the enhanced stiffness of assembly part.

Solving the rotor model in ANSYS Workbench, the modal shape of the first two natural frequencies of rotor is obtained as shown in Figure 10. It can be seen that the natural frequencies are f_1=189.03Hz, f_2 =482.74Hz, respectively. The results are very close to those of finite element calculation without enhanced stiffness, which verifies that the calculation results of finite element method are consistent with the results of ANSYS Workbench without considering the influence of the enhanced stiffness.

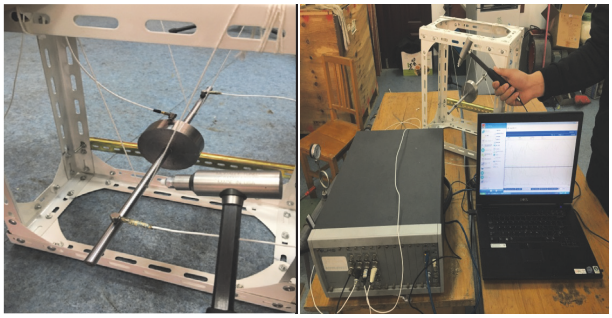

Figure 11: Modal experiment of rotor system.

4.3. Modal Experiment and Results Analysis. In order to accurately test the natural frequencies of the thick-disk rotor, the modal experiment with hammering method is done by using LMS Test.Lab. The modal experiment system is shown in Figure 11. The rotor is suspended by a set of bungees to simulate the free-free boundary conditions of the rotor, and the acceleration sensors are fixed on the different positions of the rotor surface (total 30 points). In order to ensure the validity of the amplitude signal and reduce the measurement error, each point is hammered three times, and the average value is adopted to obtain the excitation spectrum of the rotor.

The natural frequencies of modal experiment of the thick-disk rotor are shown in Figure 12, the horizontal coordinate represents the frequency range, the longitudinal coordinate represents the response amplitude, and o, f, v, and d represent the response points of the excitation. In Figure 12, o indicates the mechanical and electrical instability, f indicates the frequency stability, v indicates the pole vector stability, d indicates the damping and frequency stability, and s indicates that the three parameters are stable. And the first two natural frequencies of the rotor obtained by modal experiment are f_1=198.83Hz and f_2=503.58Hz.

The first two natural frequencies of thick-disk rotor with interference fit obtained by different methods are shown in Table 3. Comparing the natural frequencies of different methods, the influence of enhanced stiffness on natural frequencies of thick-disk rotor is very obvious, and the percent errors of natural frequencies with or without enhanced stiffness are about 5.32% and 3.16% in finite element calculation. The results without enhanced stiffness by finite element calculation with 9 nodes are very close to those of rotor with shaft and single mass point in ANSYS Workbench. The percent errors of the first two natural frequencies are down to 0.02% and 0.77%. The results with enhanced stiffness by finite element calculation with 11 nodes are close to those of 3D model in ANSYS Workbench with contact stiffness 0.01. When the contact stiffness is 0.1, the first two natural frequencies are f_1=203.31Hz, f_2 =499.39Hz. The results of modal experiment are close to the results with enhanced stiffness. The first two natural frequencies approach the results of 3D solid model in ANSYS Workbench, the contact

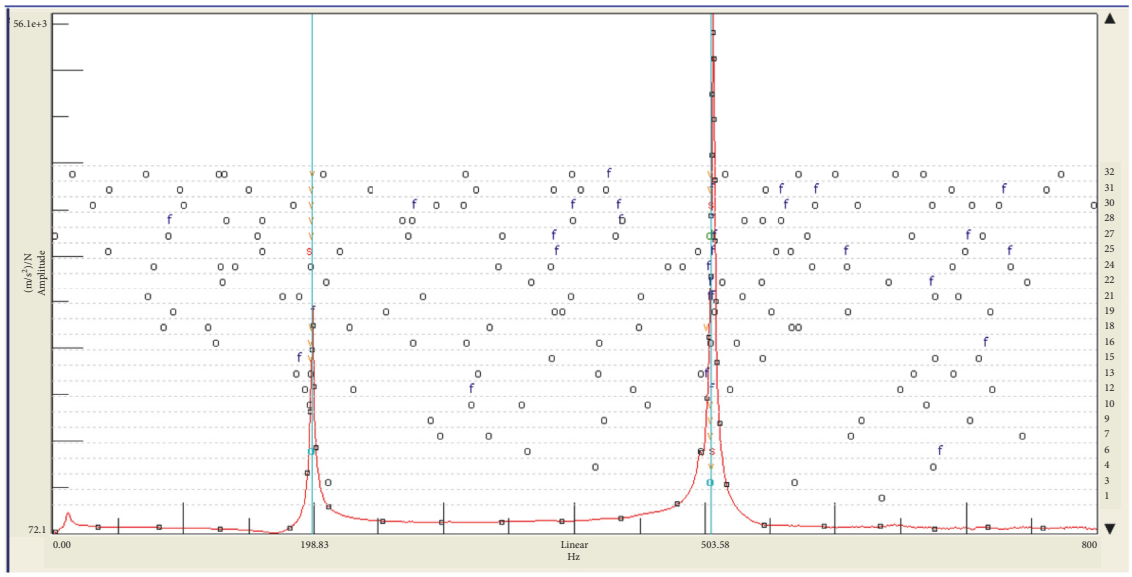

Figure 12: Natural frequencies of modal experiment.

Table 3: Natural frequencies of rotor by different methods.

Order	Finite element calculation 9 nodes	Finite element calculation 11 nodes	ANSYS Workbench 3D solid model Contact stiffness		ANSYS Workbench Shaft with point mass	Modal experiment
			0.01	0.1		
1	189.07Hz	199.13Hz	199.47Hz	203.31Hz	189.03Hz	198.83Hz
2	479.07Hz	494.20Hz	494.99Hz	499.39Hz	482.74Hz	503.58Hz

stiffness of which is 0.1, 0.01, respectively. And the error percent is down to 0.32% and 0.84%. The variation of contact stiffness is caused by the deformation of rotor under different modes.

5. Conclusions

In this paper, the enhanced coefficient of stiffness for thick-disk rotor with interference fit is firstly put forward, which is deduced based on elastic theory, and the natural frequencies of thick-disk rotor with enhanced stiffness are calculated using finite element method. In addition, the modal analysis of thick disk is performed by ANSYS Workbench and experiment to verify the accuracy of calculation results, and the following conclusions are obtained.

(i) For the thick-disk rotor with interference fit, the width of thick disk has obvious effect on the stiffness of shaft, and the enhanced coefficient of stiffness can be deduced according to elastic theory, which depends on the parameters such as friction coefficient, yield stress, Young's modulus, $\overline{D}$, $\overline{B}$, $\overline{C}$, etc.

(ii) The influence of enhanced stiffness on natural frequencies of thick-disk rotor is very obvious, and the percent errors of natural frequencies with or without enhanced stiffness are about 5.32% and 3.16% in finite element calculation.

(iii) The finite element calculation results without enhanced stiffness are very close to those of model composed of shaft and single mass point in ANSYS Workbench, and the results with enhanced stiffness are consistent with the 3D model in ANSYS Workbench and experiment.

Data Availability

The data used to support the findings of this study are included within the article.

Conflicts of Interest

The authors declare that there are no conflicts of interest regarding the publication of this paper.

Acknowledgments

This research has been supported by China Postdoctoral Science Foundation (2015M582112), Key Research and Development Project of Shandong Province (2017GGX203005), and Qingdao Postdoctoral Application Research Project (2014). The support is gratefully acknowledged.

References

[1] H. D. Nelson and J. M. McVaugh, "The dynamics of rotor-bearing systems using finite elements," *Journal of Engineering for Industry*, vol. 98, no. 2, pp. 593–600, 1976.

[2] E. S. Zorzi and H. D. Nelson, "Finite element simulation of rotor-bearing systems with internal damping," *Journal of Engineering for Gas Turbines and Power*, vol. 99, no. 1, pp. 71–76, 1977.

[3] D.-M. Ku, "Finite element analysis of whirl speeds for rotor-bearing systems with internal damping," *Mechanical Systems and Signal Processing*, vol. 12, no. 5, pp. 599–609, 1998.

[4] M. Kalita and S. K. Kakoty, "Analysis of whirl speeds for rotor-bearing systems supported on fluid film bearings," *Mechanical Systems and Signal Processing*, vol. 18, no. 6, pp. 1369–1380, 2004.

[5] M. Chouksey, J. K. Dutt, and S. V. Modak, "Modal analysis of rotor-shaft system under the influence of rotor-shaft material damping and fluid film forces," *Mechanism and Machine Theory*, vol. 48, no. 1, pp. 81–93, 2012.

[6] C.-W. Lee, D.-J. Han, J.-H. Suh, and S.-W. Hong, "Modal analysis of periodically time-varying linear rotor systems," *Journal of Sound and Vibration*, vol. 303, no. 3-5, pp. 553–574, 2007.

[7] Y. A. Khulief, F. A. Al-Sulaiman, A. Arif, R. Ben-Mansour, A. Al-Qutub, and M. Anis, "Computational Tradeoff in Modal Characteristics of Complex Rotor Systems Using FEM," *Arabian Journal for Science and Engineering*, vol. 37, no. 6, pp. 1653–1664, 2012.

[8] L. Forrai, "A finite element model for stability analysis of symmetrical rotor systems with internal damping," *Journal of Computational & Applied Mechanics*, vol. 1, 2000.

[9] Z. Liu and J. Wang, "Analysis of transient vibration of single-thick-disk rotor crossing two orders of critical speeds," *Beijing Hangkong Hangtian Daxue Xuebao/Journal of Beijing University of Aeronautics and Astronautics*, vol. 41, no. 11, pp. 2144–2157, 2015.

[10] H. Pan, H. Yuan, T. Zhao, and W. Yang, "Sensitivity Analysis of Wheel Quality and Location on Rotor Critical Speed," *Zhendong Ceshi Yu Zhenduan/Journal of Vibration, Measurement and Diagnosis*, vol. 37, no. 3, pp. 532–538, 2017.

[11] F. I. T. Petrescu, A. Apicella, A. Raffaella et al., "Something about the mechanical moment of inertia," *American Journal of Applied Sciences*, vol. 13, no. 11, pp. 1085–1090, 2016.

[12] S.-Y. Chen, C. Kung, and J.-C. Hsu, "Dynamic analysis of a rotary hollow shaft with hot-fit part using contact elements with friction," *Transactions of the Canadian Society for Mechanical Engineering*, vol. 35, no. 3, pp. 461–474, 2011.

[13] Z. Huang, B. Han, and Y. Zhou, "Modal analysis of the flexible rotor system of magnetic levitation motors under nonlinear contact," *Zhongguo Dianji Gongcheng Xuebao/Proceedings of the Chinese Society of Electrical Engineering*, vol. 34, no. 15, pp. 2438–2444, 2014.

[14] T. Kim, I. Park, and U. Lee, "Forced Vibration of a Timoshenko Beam Subjected to Stationary and Moving Loads Using the Modal Analysis Method," *Shock and Vibration*, vol. 2017, 2017.

[15] M. H. Jalali, M. Ghayour, S. Ziaei-Rad, and B. Shahriari, "Dynamic analysis of a high speed rotor-bearing system," *Measurement*, vol. 53, pp. 1–9, 2014.

[16] G. I. Giannopoulos, S. K. Georgantzinos, and N. K. Anifantis, "Coupled vibration response of a shaft with a breathing crack," *Journal of Sound and Vibration*, vol. 336, pp. 191–206, 2015.

[17] Y. T. Ai, X. Zhai, Z. Wang, and Y. L. Qiao, "Influences of normal contact stiffness on an assembly's vibration modes," *Journal of Vibration & Shock*, 2012.

[18] Y. Zhang, Z. Du, L. Shi, and S. Liu, "Determination of Contact Stiffness of Rod-Fastened Rotors Based on Modal Test and Finite Element Analysis," *Journal of Engineering for Gas Turbines and Power*, vol. 132, no. 9, p. 094501, 2010.

[19] H. Ding and L. Xiao, "The strength analysis of rotor sleeve and PM for high-speed electrical machine," *Advanced Materials Research*, vol. 338, pp. 477–480, 2011.

[20] A. Özel, Ş. Temiz, M. D. Aydin, and S. Şen, "Stress analysis of shrink-fitted joints for various fit forms via finite element method," *Materials and Corrosion*, vol. 26, no. 4, pp. 281–289, 2005.